Evolution and control of oxygen order in a cuprate superconductor

Nicola Poccia[1], Michela Fratini[1], Alessandro Ricci[1], Gaetano Campi[2], Luisa Barba[3], Alessandra Vittorini-Orgeas[1], Ginestra Bianconi[4], Gabriel Aeppli[5] and Antonio Bianconi[1]★

The disposition of defects in metal oxides is a key attribute exploited for applications from fuel cells and catalysts to superconducting devices and memristors. The most typical defects are mobile excess oxygens and oxygen vacancies, which can be manipulated by a variety of thermal protocols as well as optical and d.c. electric fields. Here we report the X-ray writing of high-quality superconducting regions, derived from defect ordering[1], in the superoxygenated layered cuprate, La$_2$CuO$_{4+y}$. Irradiation of a poor superconductor prepared by rapid thermal quenching results first in the growth of ordered regions, with an enhancement of superconductivity becoming visible only after a waiting time, as is characteristic of other systems such as ferroelectrics[2,3], where strain must be accommodated for order to become extended. However, in La$_2$CuO$_{4+y}$, we are able to resolve all aspects of the growth of (oxygen) intercalant order, including an extraordinary excursion from low to high and back to low anisotropy of the ordered regions. We can also clearly associate the onset of high-quality superconductivity with defect ordering in two dimensions. Additional experiments with small beams demonstrate a photoresist-free, single-step strategy for writing functional materials.

Illumination-induced structural transitions[4–7] are key phenomena in all the sciences, from photosynthesis in biology to photodoping[8] in semiconductor physics. Transition metal oxides, including both superconducting cuprates[9–15] and manganites[16] with their multiplicity of charge, orbital and spin-ordered states[17,18], also exhibit such transitions. In particular, photo-switching occurs in YBa$_2$Cu$_3$O$_{6+y}$ and La$_2$CuO$_{4+y}$, with mobile oxygen ions, but the microscopic mechanism is not clear[9–15]. Although there have been several efforts to study photoconductivity and its microscopic origin in cuprates, direct structural measurements of the photo-induced redistribution of mobile oxygen interstitials (i-O) are lacking. Our present X-ray measurements fill this experimental gap, allowing us to correlate nano- and microscale structural configurations with material functionality (superconductivity) and to control these configurations to create new microstructures.

La$_2$CuO$_{4+y}$ is converted from a Mott insulator to a high-temperature superconductor (HTS) by inserting i-O into the rocksalt La$_2$O$_2^R$ layers intercalated between the superconducting CuO$_2$ planes forming both random glassy and crystalline Q2 phases[1]. At optimum doping, after long annealing, the system reaches a stationary state of scale-free organization of the Q2 grains. The i-O are mobile because of a 4% tensile lattice microstrain in the spacer La$_2$O$_2^R$ layers due to its natural misfit with the superconducting CuO$_2$ planes[19,20]. Even though they are responsible for

the appearance of high-quality superconductivity, the dynamics of i-O ordering are unknown. Understanding these domain growth dynamics[21,22] will allow the definition of photopatterning protocols for La$_2$CuO$_{4+y}$ itself as well as providing the basic principles for the organization of oxygen defects in layered transition metal oxides.

Because of their obvious relevance to photolithography, we focus here on persistent effects, meaning those, such as an increase of T_c, which survive after photostimulation ends. First, we show that the persistent effects in La$_2$CuO$_{4+y}$ single crystals are due to photo-stimulated i-O mobility, and second, we give a detailed quantitative description of the photoinduced non-equilibrium disorder-to-order transition of i-O in the spacer layers. For our X-ray annealing experiments, the sample is maintained at temperatures T with $220 < T < 300$ K (refs 1,23,24) so that the full growth and coarsening process can be observed within a reasonable measuring time (approximately 15 h); in the dark or at lower T, i-O ordering takes place on timescales of weeks and months, meaning that it could not be sensibly studied. The disordered i-O phase was obtained by quenching the sample from 370 K (above the order-to-disorder transition critical temperature 330 K) to below 300 K. We measured the disorder-to-order transition of i-O domains by a novel approach using an X-ray continuous flux for photo-switching the transition at the Trieste synchrotron radiation facility Elettra. The technique allows structural investigation by X-ray diffraction (XRD) of the same portion of the sample illuminated by X-rays, as shown in Fig. 1.

We establish (Fig. 1a) the photo-induced structural effects in the illuminated area by measuring the time evolution of the XRD pattern recorded by a charge-coupled device (CCD) area detector. The reciprocal-space image reveals satellites, disappearing above the order-to-disorder transition temperature for i-O at 330 K, and associated with the three-dimensional Q2 superstructure of the i-O dopants, displaced from the main crystal reflections (004) (006) (008) of the orthorhombic *Fmmm* crystal structure by the wave-vector $\mathbf{q}_2(0.09a^*, 0.25b^*, 0.5c^*)$. We monitor the i-O ordering by recording the Q2 satellite peaks as a function of time t after rapidly quenching the sample from the high-temperature disordered phase at 370 K. Figure 1b,c shows our key experimental discovery, namely, that for a constant photon flux the intensity of the Q2 X-ray satellite reflections undergoes a nonlinear rise with t. Therefore, as for YBa$_2$Cu$_3$O$_{6+y}$ (refs 14–16), there is an increase of i-O mobility in La$_2$CuO$_{4+y}$, induced by the continuous X-ray photon flux, increasing the disorder-to-order conversion rate of the non-equilibrium annealing process by at least two orders of magnitude. Furthermore, the satellite reflections become

[1]Department of Physics, Sapienza University of Rome, P. le A. Moro 2, 00185 Rome, Italy, [2]Institute of Crystallography, CNR, via Salaria Km 29.300, Monterotondo Stazione, Roma I-00016, Italy, [3]Elettra Sincrotrone Trieste, Strada Statale 14-km 163,5, AREA Science Park, 34149 Basovizza, Trieste, Italy, [4]Department of Physics, Northeastern University, 360 Huntington Ave., Boston, Massachusetts 02115, USA, [5]London Centre for Nanotechnology and Department of Physics and Astronomy, University College London, 17-19 Gordon Street, London WC1H 0AH, UK. *e-mail: antonio.bianconi@uniroma1.it.
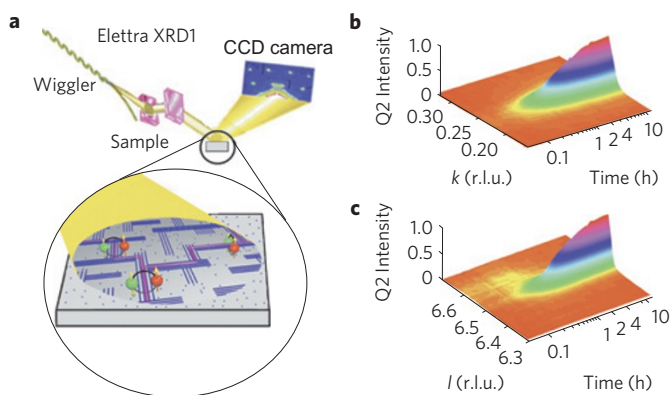
Figure 1 | X-ray photoinduced i-O ordering experiment. a, The X-ray beam emitted by the wiggler source is focused on the sample surface at the XRD beamline (XRD1) at the Elettra (Trieste) synchrotron radiation facility. A CCD area detector records the X-ray reflections from the illuminated sample area and a surface layer of about 1.5 μm thickness. The striped Q2 domains are photo-switched in the same surface layer thickness of the sample. **b,c** show the Q2 peak profiles along the in-plane k-direction (**b**) and the out-of-plane l-direction (**c**) as a function of the X-ray exposure time at constant X-ray photon flux $\Phi_{P(0.1\,nm)} = 5 \times 10^{14} N_{P(0.1\,nm)}$ s^{-1} cm^{-2} and fixed temperature 250 K, starting from the quenched disordered i-O phase with suppressed Q2 satellite reflections. There is clear evidence for both a time threshold before the i-O ordering process starts and also for the lack of saturation of the intensity growth after 14 h.

prominent only after an incubation time t_0, which is a clear indication of the nucleation and growth phenomena typical for electrically switched[2,3] and photo-induced disorder-to-order phase transitions[4–6] seen for heterostructures at the atomic limit, such as the cuprates[19].

Nucleation and growth phenomena have been much studied in three-dimensional systems. La$_2$CuO$_{4+y}$ offers an unprecedented host for their observation in a layered system because all the characteristics—notably widths and intensities—of the Q2 peaks are easily determined using synchrotron XRD. Figure 2 shows the outcome of quantitative analysis to establish the integrated Q2 intensities $\langle I \rangle$ (Fig. 2a), which measure the total volume of Q2 ordered regions, and their widths, inversely proportional to their typical extents (Fig. 2b) in all three spatial directions. Figure 2a shows the domain growth dynamics has a threshold time before which appreciable change is visible in the integrated intensity; as detailed in the Supplementary Information, the data deviate from the standard Kolmogorov formula $\langle I(t) \rangle = (1 - e^{-(t/\tau)^4})$ for nucleation and growth. Figure 2c shows how the superconducting T_c evolves with the same photo-assisted anneal, allowing correlation with the status of the nucleation and growth. Q2 order and optimal superconductivity develop via a multistage process: (1) at $t = 0$, there are very small and fairly isotropic regions of Q2 order, extending roughly $a/(\pi \cdot \text{FWHM}) \approx 2.5$ nm along both in-plane directions (a axis = 0.536 nm, b axis = 0.542 nm) and 4 nm along the c axis (1.313 nm). From $t = 0$ to just before the waiting time t_0 the Q2 regions grow visibly only in the in-plane direction and there is a negligible increase in the overall volume occupied. (2) Just at t_0, there is a very rapid rise in $\langle I \rangle$ even though the dimensions of the clusters continue to grow smoothly and relatively slowly. Therefore, at this point we are passing from the conventional coarsening regime[21], dominated by short range interactions within the two-dimensional planes, into a rapid growth phase (grey) where long range strain fields generated by the clusters bias the system towards the growth of more nuclei[2,3]. (3) After the sudden strain-induced increase in cluster growth, they begin to grow perpendicular to the planes as they continue to accrete within the planes. Well within this (yellow) regime, they actually
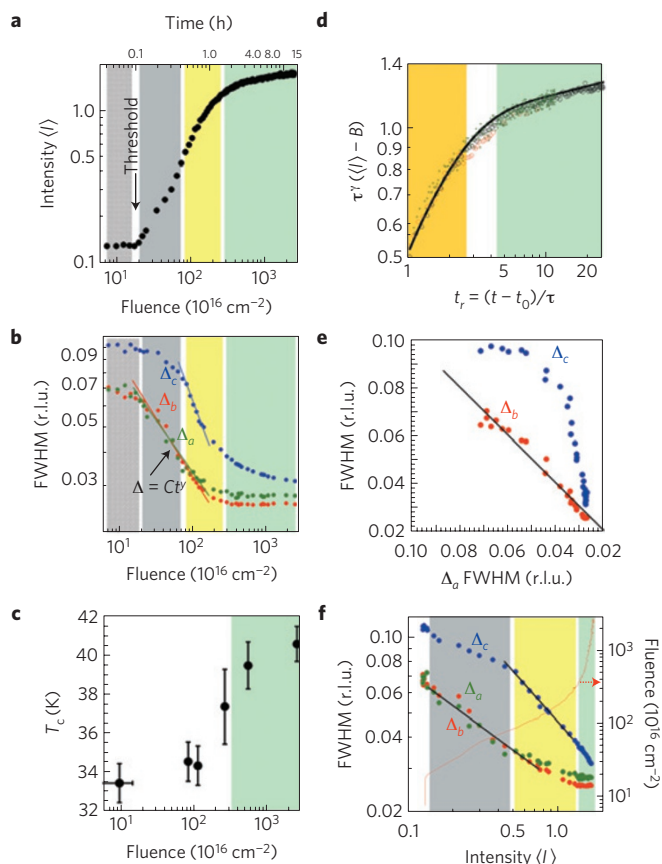
Figure 2 | The nonlinear growth dynamics. a, The integrated intensity $\langle I \rangle$ of the Q2 XRD reflections is plotted as function of fluence ϕ and time t. After an incubation period, $t < t_0$, we first see a nucleation regime (grey) where the XRD intensity increases rapidly with the growth of two-dimensional in-plane i-O ordered domains, followed by the growth of a three-dimensional order with a slow (yellow) and very slow (green) growth, lasting for at least 15 h of exposure. **b,** The full-width at half-maximum (FWHM) in reciprocal lattice units (r.l.u.) of the Q2 satellite reflections along the a axis, b axis and c axis, respectively, Δ_a, Δ_b and Δ_c, are plotted. For the regime shown in green the FWHM along the a and b axes saturates whereas in the c axis direction it continues to decrease. **c,** The superconducting critical temperature T_c of quenched samples at different times in the annealing process. The error bars indicate the divergence between the T_c onset and the maximum of the derivative of surface resistivity. **d,** The time evolution of the Q2 XRD intensity in the slow 3D growth regime can be fitted by a single curve that allows the scaling of experiments run at different temperatures in the range 250–300 K and different photon flux values. All the experimental curves, with different threshold t_0 and τ, collapse on the same curve $\tau^\gamma (\langle I(t) \rangle - B) \propto (1 - e^{-t_r}) \cdot (t_r)^\gamma$, where $t_r = (t - t_0)/\tau$ and τ is a characteristic time constant at the onset of the 3D ordering regime (yellow in **a**) and B is the background at $t = 0$. **e,** The evolution of the FWHM of the profile of XRD satellites along the b and c direction Δ_b, Δ_c of the Q2 superstructure around the (006) main reflection as a function of the FWHM, Δ_a, of the profile of the satellite in the a direction. **f,** The evolution of the FWHM of the profile of XRD satellites along the a, b and c direction, Δ_a, Δ_b and Δ_c, of the Q2 superstructure around the (006) main reflection as a function of the intensity of the superstructure reflections.

start to grow faster along c than along a and b. Finally, (4), a regime (green) is entered in which the growth is almost exclusively along the c axis, resulting, in the long-time limit, in clusters with nearly the same anisotropy as we began with at $t = 0$, but with spatial extents approximately three times larger along each direction. It is once the

in-plane growth has completed, but before the clusters have reached their full extent along c, that the superconducting T_c undergoes its most pronounced rise[23,24]. The implication is that the optimal superconductivity is associated with i-O ordering-induced Fermi surface reconstruction and electron hopping between layers[25].

The images in the right hand column of Fig. 2 show several key features of the Q2 nucleation and growth process. The first (Fig. 2a) concerns its defining functional form and universality. Here, we have carried out the experiment of Fig. 1 for several photon beam fluxes and constant sample temperatures T_s between 220 and 300 K, and consistently found the same waiting time phenomenon, characterized by the delay time t_0, which is simply proportional to the flux and approaches zero (within our measurement capability) as T_s approaches 330 K.

Figure 2d shows that domain growth data in the growth regimes (3) and (4), collected at different temperatures and with different photon fluxes, all collapse onto the same curve. The integrated intensity follows the simple functional form $\langle I(t) \rangle - B = C \cdot (1 - e^{-(t-t_0)/\tau}) \cdot (t-t_0)^\gamma$, where $t = F_{p(0.1\,\text{nm})}/\Phi_p$ and B is the intensity at $t = 0$. Here τ and t_0, which scale with $t_0 = (1/3)e^{\tau/300}$, characterize the domain growth regime in the c direction.

One of our most remarkable results is finding that the evolution of the anisotropy of the Q2 clusters proceeds from small and essentially isotropic clusters at $t = 0$ to large and essentially isotropic clusters as $t \to \infty$, via intermediate states characterized by much higher anisotropy. The growth process follows Ostwald's rule of stage states[26], where the parent phase first transforms to the metastable phase (with more oblate Q2 clusters) closest to it in free energy, as for transitions between the amorphous and crystalline phase[27] and in protein crystal growth[28]. Figure 2e shows this excursion, where we treat the in-plane width Δ_a as the control parameter. The independently measured in-plane width Δ_b is indistinguishable from Δ_a, and therefore falls on the diagonal, whereas Δ_c approaches the diagonal along horizontal and vertical straight lines, respectively, for the small and large cluster limits corresponding to large and small Δ_a.

An important problem in the non-equilibrium physics of first-order phase transitions is to establish the relative importance of nucleation and growth[3]. A particularly simple analysis tool is a plot of the widths corresponding to the sizes of the ordered clusters against the integrated intensity $\langle I \rangle$, reflecting the total volume occupied by the ordered phase. Figure 2f is such a plot for our data and reveals the different growth regimes. In particular, we see that the Q2 peak widths in the regime before the threshold time t_0 are actually growing much faster than $\langle I \rangle$, implying that, initially, different ordered regions are simply combining, leaving the net Q2 volume essentially unchanged. Immediately after t_0, the Q2 widths follow a power law $\Delta = \langle I \rangle^{-\alpha}$, with exponents $\alpha_a \approx \alpha_b \approx 0.39 \pm 0.02$ and $\alpha_{c(I)} = 0.2 \pm 0.02$. The in-plane exponents are difficult to distinguish, but the c axis exponent is much smaller. Furthermore, the sum of the three exponents is indistinguishable from unity, indicating that the rising volume fraction of Q2 ordered regions is controlled by the in-plane growth of pre-existing clusters. On the other hand, for times well beyond t_0, we enter a regime (yellow) where α_a and α_b remain unchanged but $\alpha_{c(II)} = 0.65 \pm 0.02$ is very much higher. The exponents now sum to appreciably more than unity, meaning that this is a growth and agglomeration regime, where clusters are merging (particularly along c) as well as growing, thus adding to the total volume fraction of Q2 ordered regions at a smaller rate than in a pure, independent cluster, growth regime. In the final growth regime (green), the size of the Q2 grains reaches a maximum size and the reflection profile in the b and a directions reaches saturation whereas the FWHM of reflections in the c direction decreases with a power law exponent $\alpha_{c(III)} = 0.89 \pm 0.15$, an exponent close to unity, implying growth of the ordered phase mainly by further growth of existing clusters along the c axis.
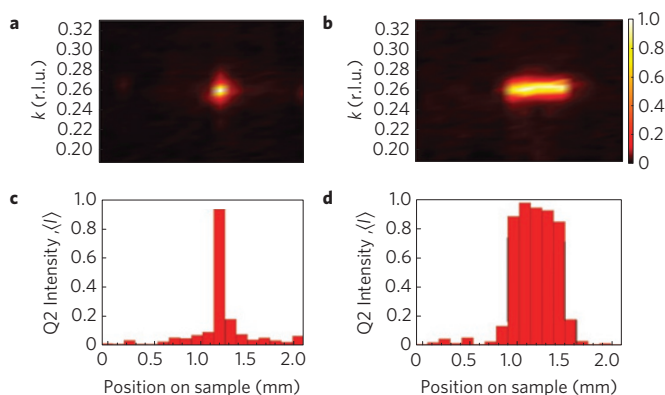
Figure 3 | X-ray manipulation of high-T_c superconductors. a,b, The formation of a dot and of a stripe of Q2 i-O fractal phase embedded in the disordered phase. A surface spot was illuminated by the X-ray beam for a time greater than $t_0 + 2\tau$ with a X-ray fluence well above the threshold at a constant temperature of 250 K. As a result, the fractal i-O phase was formed in the illuminated portion of the sample surface, as shown in Fig. 1, whereas in the masked part the i-O were in the disordered phase. Subsequently we read the sample surface using a low X-ray flux beam, below the threshold for non-invasive XRD. The lower figures show 3D colour plots of the XRD Q2 satellite reflection. **c,d,** The integrated intensity is plotted as a function of the position of the beam on the sample, showing the formation of the 100 μm dot and the stripe. The dot and the stripe can be easily erased by locally increasing the sample temperature above 350 K. This technique allows one to switch (on–off) the self-organized microstructures on a nanometre scale and to control them *in situ* by synchrotron X-ray scattering.

Although each regime in Fig. 2f is clearly unique, it is worth repeating that a common feature is that the sum $\alpha_a + \alpha_b + \alpha_c$ of the exponents is never less than unity (within error), implying that there is never any need for new nuclei for Q2 ordered regions beyond those which exist after the quench. The entire process by which $\langle I \rangle$ increases is accounted for by growth and agglomeration of pre-existing nuclei.

Having extensively characterized the non-equilibrium disorder-to-order process induced by X-ray irradiation, we show here that the observed phenomena can be exploited for writing and reading Q2 patterns, leading to possible technological applications for writing and erasing planar superconducting electronic devices. We have followed a multistep protocol, starting by warming the sample to 380 K, where the Q2 peaks disappear entirely (erasing). The sample is then quenched down to 200–300 K and illuminated at a constant temperature. At this point it is possible to write patterns such as the dot in Fig. 3a or the stripe in Fig. 3b using a photon beam size of 100 μm with flux of 10^{15} photons cm^{-2}. In fact, under continuous illumination the Q2 superstructure peak is formed owing to the photo-conversion of the i-O disordered phase to the i-O scale-free ordered phase. These results clearly show that it is possible to read and write microstructures, with edges defined to within at least the 100 μm step size in our current demonstration experiments, formed by two different superconducting materials, namely the first with disordered i-O and the second with scale-free ordered i-O in the spacer layers, as shown in Fig. 3.

As $t \to \infty$, the FWHM of the i-O peaks remains at the relatively high value of 0.025 reciprocal lattice units (r.l.u.), which imposes a very small lower bound of $a/(\pi \cdot \text{FWHM}) \approx 6$ nm on the possible resolution of future nanolithography employing advanced, highly focused X-ray beams. It is also worth noting that X-rays can be used in combination with photons of other wavelengths to cause disorder-to-order phase transitions in the recording material, in analogy with optical CD data recording. In particular, for

erasure, the necessary increase of the sample temperature above the disorder-to-order transition can be achieved *in situ* by means of higher flux laser illumination or microwave beam irradiation. The lowest level of X-ray photon flux (below the threshold) can be used to check the Q2 pattern without damaging the superconductor surface. An initial device could be manufactured by simply drawing a wire of Q2 domains across the sample by continuous translation of the sample stage under an X-ray beam defined by modern focusing optics exploiting a Fresnel zone plate. Midway through the wire drawing process, the fluence is reduced below its critical value for Q2 formation by either a brief acceleration of the stage or closing off the beam with a shutter, leaving behind the desired weak link. The stage can be manipulated to produce more complex circuits, including wire loops containing weak links, and the stability, for periods of weeks, of the disordered phase at room temperature in the absence of radiation assures the possibility of moving a prepared circuit from the lithography station to an electrical measuring cryostat remote from the X-ray source. We note also the possibility of patterning not only with X-rays, but also with electron beam writers, which are much more common and routinely produce smaller beams.

Given that electronic inhomogeneities are the prerequisite for interesting multi-terminal devices such as transistors and tunnel junctions, our results open the way to novel superconducting electronics and their manipulation. Moreover, the control and manipulation through x-ray excitation of i-O or vacancies organization can also be used to modulate complexity and write devices in manganites[5,16–18] and at the interfaces of functional oxide superlattices.

Methods

The XRD experiment uses a photon beam of monochromatic, 0.1 nm wavelength (12.4 keV) X-rays emitted from the 2 GeV electron storage ring Elettra at Trieste. The X-ray beam spot on the sample surface has dimensions in the range between 400×400 and $100 \times 100\,\mu m^2$. The intensity, I(Q2), of the superstructure satellites due to the Q2 ordering of (i-O) in the $La_2CuO_{4.1}$ crystal is integrated over square sub-areas of the images recorded by the CCD detector and then normalized to the intensity (I_0) of the tail of the main crystalline reflections. The synchrotron X-ray photons are focused to a spot size of 100–400 μm on the sample surface with a flux (defined as the number of photons hitting the sample surface per second per unit area) of $\Phi_{P(0.1\,nm)} = f \times 10^{14} N_{P(0.1\,nm)}\,s^{-1}\,cm^{-2}$, where f can be controlled and varied in the range $1 < f < 10$. For a typical case, where $f = 5$, the power density on the sample surface is $1\,W\,cm^{-2}$, equivalent to an optical (510 nm) laser flux of $\Phi_{P(510\,nm)} = 2.5 \times 10^{18} N_P\,s^{-1}\,cm^{-2}$, as shown in Fig. 1. The X-ray penetration depth is about 1.5 μm, implying an illuminated areal density of Cu ions of the order of $10^{18}\,cm^{-2}$. Considering that an energy of 2 eV is required to create an electron–hole pair in cuprates, this X-ray flux can induce photo-induced persistent effects in a micrometre thick layer much like those that visible lasers induce in much thinner films[11–16]. The effect of continuous illumination corresponds to photo-excitation in which the state-changing rate is proportional to the intensity of light. Therefore the physical state of the system is controlled by the fluence $F_{P(0.1\,nm)}(N_{P(0.1\,nm)} \cdot cm^{-2}) = \Phi_P \cdot t$; we have checked that on doubling or halving the flux, the timescales are respectively halved or doubled.

References

1. Fratini, M. *et al.* Scale-free structural organization of oxygen interstitials in La_2CuO_{4+y}. *Nature* **466,** 841–844 (2010).
2. McWhan, D. B., Aeppli, G., Remeika, J. P. & Nelson, S. Time-resolved X-ray scattering study of BaTiO₃. *J. Phys. C* **18,** L307 (1985).
3. Littlewood, P. B. & Chandra, P. Delayed nucleation at a weakly first-order transition. *Phys. Rev. Lett.* **57,** 2415–2418 (1986).
4. Nasu, K. *Photoinduced Phase Transitions* (World Scientific, 2004).
5. Tokura, Y. Photoinduced phase transition: A tool for generating a hidden state of matter. *J. Phys. Soc. Jpn* **75,** 011001 (2006).
6. Kawamoto, T. & Abe, S. Photoinduced phase transition accelerated by use of two-component nanostructures: A computational study on an Ising-type model. *Phys. Rev. B* **68,** 235112 (2003).
7. Bougrioua, F. *et al.* Light-induced layer by layer thickening in photosensitive liquid crystal membranes. *Phys. Rev. Lett.* **95,** 027802 (2005).
8. Soh, Y-A., Aeppli, G., Zimmermann, F. M., Isaacs, E. D. & Frenkel, A. I. X-ray induced persistent photoconductivity in Si-doped $Al_{0.35}Ga_{0.65}As$. *J. Appl. Phys.* **90,** 6172–6176 (2001).
9. Nieva, G. *et al.* Photoinduced enhancement of superconductivity. *Appl. Phys. Lett.* **60,** 2159–2161 (1992).
10. Lederman, D., Hasen, J., Schuller, I. K., Osquiguil, E. & Bruynseraede, Y. Photoinduced superconductivity and structural changes in high temperature superconducting films. *Appl. Phys. Lett.* **64,** 652–654 (1994).
11. Kudinov, V. I. *et al.* Persistent photoconductivity in $YBa_2Cu_3O_{6+x}$ films as a method of photodoping toward metallic and superconducting phases. *Phys. Rev. B* **47,** 9017–9028 (1993).
12. Hoffmann, A. *et al.* Persistent photoinduced superconductivity. *J. Alloys Compounds* **251,** 87–93 (1997).
13. Fainstein, A., Maiorov, B., Guimpel, J., Nieva, G. & Osquiguil, E. Annealing disorder and photoinduced order of oxygen chains in detwinned $YBa_2Cu_3O_{6.65}$ single crystals probed by Raman scattering. *Phys. Rev. B* **61,** 4298–4304 (2000).
14. Bahrs, S. *et al.* Light-induced oxygen-ordering dynamics in $(Y,Pr)Ba_2Cu_3O_7$: A Raman spectroscopy and Monte Carlo study. *Phys. Rev. B* **70,** 014512 (2004).
15. Markowitsch, W. *et al.* Persistent photoconductivity in $YBa_2Cu_3O_x$ by visible and UV excitation below T_c. *Physica C* **405,** 173–178 (2004).
16. Kiryukhin, V. *et al.* An X-ray-induced insulator–metal transition in a magnetoresistive manganite. *Nature* **386,** 813–815 (1997).
17. Dagotto, E. Complexity in strongly correlated electronic systems. *Science* **309,** 257–262 (2005).
18. Bishop, A. R. HTc oxides: A collusion of spin, charge and lattice. *J. Phys.: Conf. Ser.* **108,** 012027 (2008).
19. Agrestini, S., Saini, N. L., Bianconi, G. & Bianconi, A. The strain of CuO_2 lattice: The second variable for the phase diagram of cuprate perovskites. *J. Phys. A* **36,** 9133–9142 (2003).
20. Fratini, M., Poccia, N. & Bianconi, A. The Feshbach resonance and nanoscale phase separation in a polaron liquid near the quantum critical point for a polaron Wigner crystal. *J. Phys.: Conf. Ser.* **108,** 012036 (2008).
21. Bray, A. J. Coarsening dynamics of phase-separating systems. *Math. Phys. Eng. Sci.* **361,** 781–792 (2003).
22. Zanetti, M. in *Kinetics of Phase Transitions* (eds Puri, S. & Wadhawan, V.) 153–202 (CRC, Taylor & Francis Group, 2009).
23. Kremer, R. K. *et al.* Percolative phase separation in La_2CuO_{4+y} and $La_2Sr_xCuO_4$. *Z. Phys. B* **86,** 319–324 (1992).
24. Ahrens, E. *et al.* Thermal history-dependent superconductivity and local structure in $La_2CuO_{4+\delta}$. *Physica C* **212,** 317–322 (1993).
25. Innocenti, D. *et al.* Shape resonance for the anisotropic superconducting gaps near a Lifshitz transition: The effect of electron hopping between layers. *Supercond. Sci. Technol.* **24,** 015012 (2011).
26. Ostwald, W. *Lehrbuch der Allgemeinen Chemie* Vol. 2 (W. Engelmann, 1886).
27. Chung, S-Y., Kim, Y-M., Kim, J-G. & Kim, Y-J. Multiphase transformation and Ostwald's rule of stages during crystallization of a metal phosphate. *Nature Phys.* **5,** 68–73 (2008).
28. Streets, A. M. & Quake, S. R. Ostwald ripening of clusters during protein crystallization. *Phys. Rev. Lett.* **104,** 178102 (2010).

Author contributions

All authors contributed to providing experimental support, interpreting data and writing the manuscript. A.B., L.B., G.B., G.C., M.F., N.P., A.R. and A.V-O. performed the experiment. A.B., G.C., M.F., N.P. and A.R. performed sample manipulations. L.B. provided the X-ray beamline. N.P., G.A., G.B. M.F. and A.V-O. performed the data analysis. G.B. provided theoretical support. G.A., A.B. and N.P. wrote the paper.